ACS APPLIED NANO MATERIALS

www.acsanm.org Article

Ag_2S Quantum Dots for Use in Whole-Cell Biohybrid Catalyst for Visible-Light-Driven Photocatalytic Organic Pollutant Degradation

Peiqing Sun, Kunlun Li, Kai Lin,* Wei Wei,* and Jing Zhao*

Cite This: https://doi.org/10.1021/acsanm.2c01955 Read Online

ACCESS | Metrics & More | Article Recommendations | Supporting Information

ABSTRACT: Semiartificial photosynthetic systems have shown tremendous potential to address global energy issues by combining the exceptional optical properties of nanomaterials with biological whole-cell catalysts. To achieve sustainable energy conversion between inorganic materials and whole cells in semiartificial photosynthetic systems, it is highly desirable to introduce biocompatible nanomaterials with broad light adsorption into the hybrid catalysis system. Herein, we developed a whole-cell biohybrid catalyst with in situ synthesized Ag_2S QDs for visible-light-driven photocatalytic organic pollutant degradation. With the synthesized Ag_2S QDs on the surface of engineered *Escherichia coli* cells, the biohybrid system showed superior performance for the photocatalytic degradation of organic pollutants. The photogenerated reactive oxygen species ($^{\bullet}O_2^-$) were confirmed to play a pivotal role in removing organic pollutants during the photocatalytic process. The enhanced photocatalytic activity of the *E. coli*-Ag_2S QD biohybrid system could be ascribed to the effective separation and transfer of the interfacial charge carriers. This whole-cell biohybrid system could provide a promising approach for environmental issues in solar energy conversion.

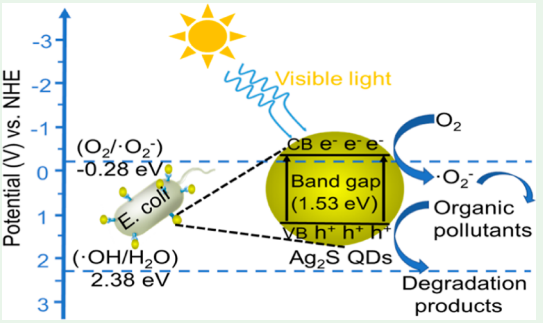

KEYWORDS: *whole-cell biohybrid catalyst, surface-display, Ag_2S QDs, photodegradation, solar energy*

1. INTRODUCTION

Solar-to-chemical conversion by semiartificial photosynthetic systems has attracted significant attention in recent years as a newly emerging approach that uses solar energy to address global energy and environmental challenges.[1−3] To this end, several excellent semiartificial photosynthetic systems have been exploited based on the different combinations of light-harvesting synthetic material and biological components, which were employed as biohybrid catalysts for their applications in different fields, such as CO_2 reduction,[4,5] H_2 evolution,[6−8] and N_2 fixation.[9−11] Among them, a significant breakthrough was made by Yang et al. who developed a semiartificial photosynthetic system based on the combination of biologically precipitated CdS nanoparticles and the non-photosynthetic bacterium *Moorella thermoacetica* for light-driven acetic acid production from carbon dioxide.[12] Honda et al. first demonstrated the semiartificial photosynthetic system by using anatase TiO_2 with an engineered *Escherichia coli* for biological hydrogen production.[13] Inspired by these seminal studies, we developed a surface-display biohybrid approach to light-driven hydrogen production in air with in situ biosynthesis of biocompatible CdS nanoparticles by engineered *E. coli* cells.[14] These results provide important guidance for the rational design of a biocompatible photosensitizer in semiartificial photosynthetic systems to address energy and environmental issues in the future.

Although semiconductor-based photocatalysts such as CdS (E_g = 2.51 eV, 405 nm) and TiO_2 nanoparticles (E_g = 3.2 eV, 300 nm) show their photocatalytic activities in semiartificial photosynthetic systems, the photodamage with increasing blue light radiation is harmful to whole cells, which leads to the low catalytic efficiency of semiartificial photosynthetic systems.[15,16] Biohybrid systems combining broad light absorption nanomaterials with whole cells in light-driven reactions could overcome these limitations. Pioneering work by Strano et al. demonstrated that the combination of single-walled carbon nanotubes with broad light absorption and chloroplast greatly improved the photosynthetic efficiency in plants.[17] Recently, Jiang, Wang, and Wong et al. reported the iodine-doped hydrothermally carbonized carbon@*E. coli* biohybrid system that showed broad light absorption ability and visible-light-enhanced hydrogen production.[8] However, the synthesis of these semiconductors still requires a complicated process. Ag_2S quantum dots (Ag_2S QDs), as excellent photosensitizers, demonstrate tremendous potential for biological applications.[18,19] Compared to narrow band gap QDs with highly

Received: May 5, 2022
Accepted: June 23, 2022

https://doi.org/10.1021/acsanm.2c01955
ACS Appl. Nano Mater. XXXX, XXX, XXX−XXX

toxic components, such as PbS,[20] CdSe/ZnS,[21] and InAs,[22] Ag_2S QDs with no toxic heavy metal components exhibited excellent biocompatibility in biomedical applications.[23,24] Notably, the significant breakthrough was made by Wang et al. who first reported the chemical synthesis of Ag_2S QDs by thermally decomposing a single-source precursor of Ag-(DDTC) $[(C_2H_5)_2NCS_2Ag]$.[25] Ag_2S-based materials have been widely in the field of photocatalysis due to their excellent and efficient photooxidative properties. Huang et al. reported that Ag_2S-deposited Cu_2O cubes forming heterostructures exhibited high photocatalytic activity for degradation of methyl orange.[26]

Inspired by these pioneering works, here, we developed a whole-cell biohybrid catalyst with the in situ synthesized Ag_2S semiconductor by using the surface-display approach in *E. coli* for further applications utilizing solar energy. Based on our previous studies,[27] two components are essential for constructing photosynthetic biohybrid systems: (1) in situ synthesized Ag_2S QDs, a biocompatible, light-harvesting component, and (2) the well-studied microorganism E. coli, engineered as a whole-cell biocatalyst.[28] By integrating the light-harvesting properties of Ag_2S QDs with the self-repairing/replicating potential of engineered *E. coli* cells, the *E. coli*-Ag_2S QD biohybrid system showed broad light absorption and exhibited excellent performance for the photocatalytic degradation of organic pollutants under visible light (Figure 1).

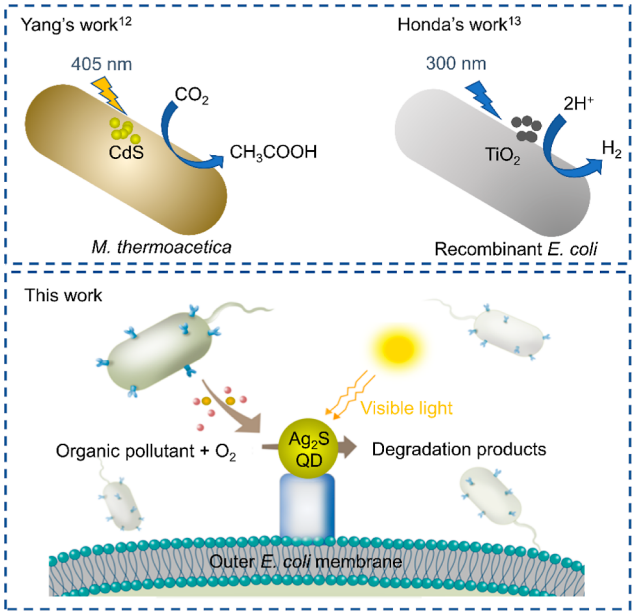

Figure 1. Schematic representation of a biohybrid system as a whole-cell biocatalyst by a surface-display approach for the photodegradation of organic pollutants under visible light irradiation.

2. EXPERIMENTAL SECTION

2.1. Construction of Plasmids for Surface-Displayed Silver-Binding Peptide on *E. coli*. According to the previously published method,[29] the expression gene of outer membrane protein A (OmpA)−silver-binding peptide fusion protein was constructed in three steps. The gene encoding OmpA, which has 159 amino acids, was amplified by the primers OmpA-1 and OmpA-2, and the genes of the full-length silver-binding peptide with the FLAG-tag at the *C*-terminus were synthesized. Two fragments were then joined together by overlapping PCR using OmpA-1 and the silver-binding peptide. After confirmation by sequencing, the PCR product was digested with BamHI and kpnI and then inserted into the pBAD vector to display the silver-binding peptide on the surface of *E. coli* cells, and the pBAD-OmpA plasmid served as a negative control. Finally, two plasmids were transformed into *E. coli* BL21(DE3).

2.2. SDS-PAGE and Western Blotting Analysis of Displayed Fusion Proteins. The *E. coli* BL21(DE3) strain containing the OmpA-silver-binding peptide plasmid and the negative control were incubated overnight in LB medium containing ampicillin (50 $\mu g\ mL^{-1}$) at 37 °C with shaking. After 1:100 dilution in LB medium, the cells were grown in LB with ampicillin (50 $\mu g\ mL^{-1}$) at 37 °C to an OD_{600} = 0.6−0.8, induced overnight by arabinose (0.002%). Cells were harvested by centrifugation (4500 rpm, 5 min) and resuspended in lysis buffer (PBS, pH 7.4). After sonication, the two fractions of the supernatant and the cell membrane were separated by centrifugation (14,000 rpm, 30 min). The cell membrane was resuspended in TDSET buffer (1% Triton X-100, 0.2% sodium deoxycholate, 0.1% SDS, 10 mM tetrasodium EDTA, and 10 mM Tris/HCl). After centrifugation (14,000 rpm, 10 min), the precipitate was resuspended in 300 μL of PBS. Then, 50 μL of the supernatant and the resuspended precipitate fractions were resuspended in loading buffer, and the samples were heated to 95 °C for 10 min. The samples were loaded on 15% SDS-PAGE gels and electrophoresed at 50 V for 30 min and then at 150 V for 50 min. For Western blotting analysis, the separated proteins were transferred onto polyvinylidene fluoride membranes (Bio-Rad) at 4 °C for 2 h (100 V, 250 mA). After blocking at room temperature for 2 h in Blotto solution (5% nonfat dry milk in 1 × TBST), a monoclonal anti-FLAG tag (1:1000, Santa Cruz Biotechnology) was added and incubated overnight at 4 °C. Horseradish peroxidase (HRP)-conjugated goat antimouse antibody (Santa Cruz Biotechnology) was used as a secondary antibody at room temperature for 2 h.

2.3. Synthesis of Ag_2S QDs. The recombinant *E. coli* strains were cultured as described above. When the OD_{600} value of the cell culture reached 0.8, 0.1 wt % L-cysteine was added to the medium. After reacting for 4 h, 1 mM $AgNO_3$ was added into the medium for a further 16 h at 37 °C for the synthesis of Ag_2S QDs.

To measure the metal ion adsorption ability of the recombinant *E. coli* strain, the silver-adsorbed cells were lyophilized to measure the dry weight and subjected to wet ashing. Then, the samples were analyzed by inductively coupled plasma-atomic emission spectrometry (ICP-AES).

2.4. Characterization of the *E. coli*-Ag_2S QD Biohybrid. The optical properties of the *E. coli*-Ag_2S QD biohybrid were analyzed by UV−Vis diffuse reflectance spectroscopy (DRS) using a Lambda 950 (PerkinElmer) spectrometer. The band gap of the obtained Ag_2S was calculated using Tauc plots. All images were obtained using field-emission transmission electron microscopy (TEM, Tecnai G2 F20 S-TWIN, FEI, USA) equipped with EDX spectroscopy. The samples were washed three times using deionized water and then dried at room temperature.

2.5. Evaluation of the Photocatalytic Activity of the *E. coli*-Ag_2S QD Biohybrid System. After silver ion adsorption, the samples were harvested by centrifugation (4000 rpm, 15 min) and then resuspended in PBS. The suspensions containing 2×10^9 cells/mL were then transferred to a cylindrical reactor (Beijing Perfectlight). For visible light irradiation, a 300 W xenon lamp (PLS-SXE300D, Beijing Perfectlight) equipped with a 420 nm cutoff filter was used as the light source. The light intensity is 1000 W m^{-2}. The solution was then shaken continuously in the dark for 30 min to ensure adsorption−desorption equilibrium between the sample and methylene blue (MB, 20 mg L^{-1}). During the irradiation experiments, the samples were collected at various times to monitor the removal of MB using a UV−Vis spectrophotometer (UV-2700, Shimadzu, Kyoto, Japan).

2.6. Identification of Reactive Oxygen Species. According to the previously described method,[30−32] free radical capture experiments were performed by adding different scavengers into the reaction system. Isopropanol (IPA), sodium oxalate, and 1,4-benzoquinone (BQ) were used as ·OH, hole, and $\bullet O_2^-$ scavengers,

https://doi.org/10.1021/acsanm.2c01955
ACS Appl. Nano Mater. XXXX, XXX, XXX−XXX

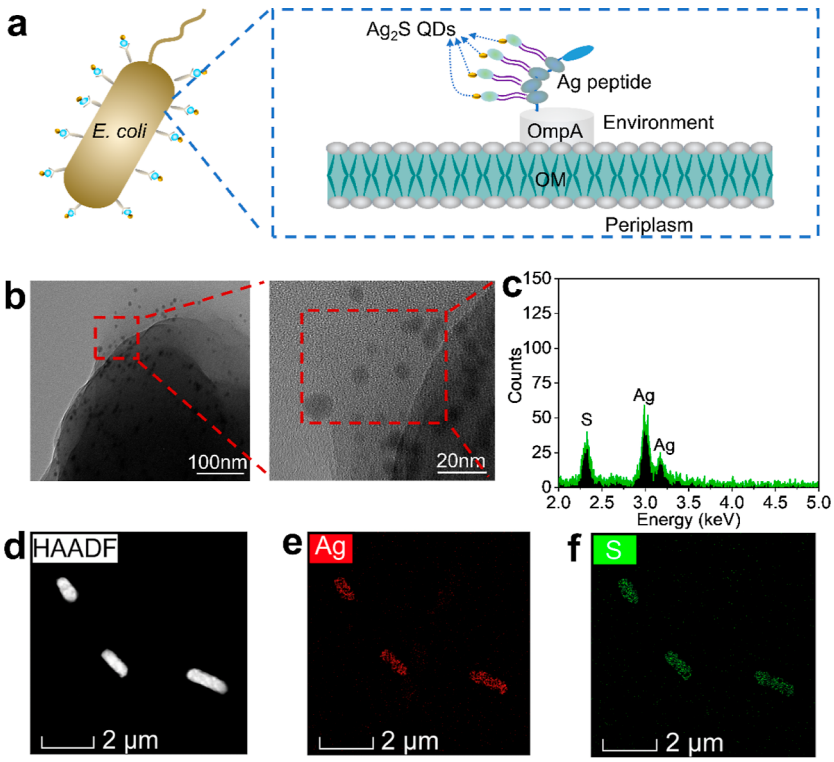

Figure 2. (a) Detailed diagram of silver-binding peptide displayed on the surface of an engineered *E. coli* cell by the outer membrane protein OmpA. (b) TEM images of the synthesized Ag_2S QDs on the surface of engineered *E. coli* cells. (c) Result of EDX analysis of the synthesized Ag_2S QDs. (d) HAADF-STEM images of the *E. coli*-Ag_2S QD biohybrid system. (e,f) EDS mapping shows the Ag and S on the surface of the entire cell. Scale bars in (b) 100 nm and 20 nm and (d–f) 2 μm.

respectively. These tests were performed following the same photocatalytic experiment as mentioned above. Electron spin resonance (ESR) tests were carried out at ambient temperature using a Bruker EMX ESR spectrometer (Billerica, MA). A 300 W xenon lamp equipped with a 400 nm cutoff filter was used as the light source. As a specific $\bullet O_2^-$ scavenger, superoxide dismutase (SOD) was used to catalyze the conversion of $\bullet O_2^-$ into O_2 in the photocatalytic degradation. ESR spectra were obtained from the *E. coli*-Ag_2S QD biohybrid system containing 20 mM DMPO before and after irradiation. All spectra were recorded after 4 min of irradiation.

3. RESULTS AND DISCUSSION

3.1. Construction and Characterization of the *E. coli*-Ag_2S QD Biohybrid. As described in previous works,[27,33] we selected a silver-binding peptide displayed on the surface of engineered *E. coli* cells for the synthesis of Ag_2S QDs (Figure 2a). The plasmid containing the fusion protein expression gene encoding the *E. coli* OmpA and a silver-binding peptide was transformed into the *E. coli* strain BL21(DE3). SDS–PAGE and immunoblotting analyses were used to analyze the expression of the surface-displayed silver-binding peptide. As illustrated in Figure S1, the expressed recombinant protein had a molecular weight of approximately 30 kDa according to SDS–PAGE gel (calculated MW = 30.2 kDa), and the identities of the proteins were further verified by immunoblot analysis with the anti-FLAG antibody. This result indicated that the silver-binding peptide was successfully displayed on the *E. coli* cell surface. Subsequently, we measured the resistance of *E. coli* with surface-displayed silver-binding peptide against silver ions. Compared to the controls (without induction or expressing only OmpA), the *E. coli* expressing silver-binding peptide showed enhanced tolerance to silver ions, and the optimal concentration of the silver ions was 50 μM (Figure S2) which is higher than that of the undisplayed samples. The toxic metals can be precipitated to form metal complexes on the cell surface due to the detoxification mechanism of *E. coli*.[34] During this process, the induced cysteine desulfhydrase in the *E. coli* can catalyze the cysteine-to-sulfide conversion, which will provide the basis for Ag_2S nanoparticle formation on the cell surface of *E. coli*. According to the optimized concentration of the silver ions, the *E. coli*-Ag_2S biohybrid system was constructed by adding 0.1 wt % cysteine to the culture medium when the value of OD_{600} reached 0.8. As a result, the color of the hybrid system turned brown, preliminarily indicating that the *E. coli*-Ag_2S biohybrid system was successfully fabricated. TEM–EDX was performed to further investigate the morphology of the hybrid. Compared to the images of *E. coli* cells alone (Figure S3), visibly dense nanoparticles were more closely deposited on the surface of *E. coli* cells, and the formed nanoparticles were observed to be smaller than 10 nm in size (Figure 2b). Moreover, the characterization of EDS confirmed that the primary elements of the surface nanoparticles were Ag and S, and the Ag/S ratio was close to 1.768:1 (Figure 2c), which was close to the theoretical stoichiometric ratio of silver sulfide. Additionally, high-angle annular dark-field scanning transmission electron microscopy (HAADF-STEM) and energy-dispersive spectrometry (EDS) mapping were carried out to reveal the surface chemical composition of the *E. coli*-Ag_2S biohybrid system. As shown in Figure 2d–f, high densities of bright spots were uniformly distributed on the surface of engineered *E. coli* cells. Thus, the results confirmed that Ag_2S nanoparticles were successfully fabricated and immobilized in the *E. coli*-Ag_2S biohybrid system. Furthermore, the optical properties of the

https://doi.org/10.1021/acsanm.2c01955
ACS Appl. Nano Mater. XXXX, XXX, XXX–XXX

obtained Ag_2S nanoparticles, such as absorption and photoluminescence spectra, are shown in Figure S4. The UV−vis DRS spectrum of Ag_2S nanoparticles showed a very broad absorption spectrum ranging from the visible light to near-infrared region (Figure S4a), implying the excellent light utilization property. Interestingly, the PL spectra exhibited near-infrared emission (around 1050 nm) under 808 nm excitation and were observed in NIR imaging (Figure S5), which was similar to that reported for Ag_2S QDs.[35] The results indicated that Ag_2S QDs were successfully synthesized by a surface-displayed silver-binding peptide on the outer membranes of engineered *E. coli* cells. In addition, the amount of synthesized Ag_2S QDs on the surface of engineered *E. coli* cells was measured by ICP−mass spectrometry and reached 0.96 ± 0.02 μg 10^8 cells after 16 h (Figure S6), which was much higher than that in cells not displaying the silver-binding peptide.[27]

3.2. Photocatalytic Activity of the *E. coli*-Ag_2S QD Biohybrid System. The photocatalytic activity of the *E. coli*-Ag_2S QD biohybrid system was characterized by measuring the removal rate of an organic pollutant under visible light irradiation. We used MB as the model organic pollutant. As shown in Figure 3a, a higher removal of MB was observed for

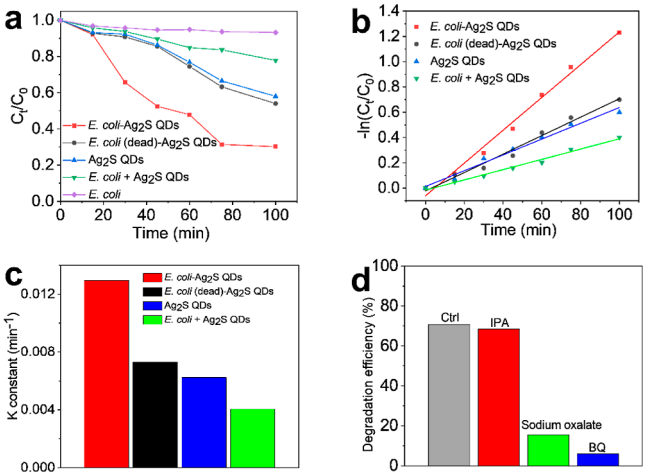

Figure 3. (a) Photocatalytic degradation and (b) kinetic fit curves for the degradation of MB over the *E. coli*-Ag_2S QD biohybrid system under visible light irradiation. (c) Corresponding rate constants. (d) Effect of scavengers on the degradation efficiency of MB over the *E. coli*-Ag_2S QD biohybrid system under visible light irradiation (5 mM IPA, 1 mM sodium oxalate, and 1 mM BQ).

the treatment of the *E. coli*-Ag_2S QD biohybrid system illuminated under the same conditions compared with other treatments. In particular, the removal efficiency reached approximately 70.8% after 100 min. Moreover, the degradation performance of the *E. coli*-Ag_2S QD biohybrid system belonged to the pseudo-first-order model (Figure 3b). The rate constant of the *E. coli*-Ag_2S QD biohybrid system was 0.0126 min^{-1}(Figure 3c), which was higher than those of controls (pristine *E. coli* or Ag_2S QDs alone).[36] This may be attributed to the outer membrane protein as an electron carrier to facilitate electron transfer in the microbial decolorization process.[37] These results demonstrated that the *E. coli*-Ag_2S QD biohybrid system was highly efficient in degrading organic pollutants under visible light.

3.3. Mechanism of Photodegradation for the *E. coli*-Ag_2S QD Biohybrid System. To explore the mechanism of the photocatalytic process mediated by the *E. coli*-Ag_2S QD biohybrid system, reactive species trapping experiments were carried out to investigate the effects of the key reactive species. IPA, BQ, and sodium oxalate were employed to capture hydroxyl radicals (·OH), superoxide radicals ($\bullet O_2^-$), and hole radicals (h^+), respectively.[38] As shown in Figure 3d, the removal rates after the addition of IPA, sodium oxalate, and BQ decreased to 68.6, 15.6, and 6.0%, respectively, suggesting that $\bullet O_2^-$ and h^+ are the dominant reactive species during the MB degradation. However, the removal rate is nearly unchanged after adding IPA to the photocatalytic reaction compared to the *E. coli*-Ag_2S QD biohybrid system with no scavenger, suggesting that ·OH is not the primary reactive species in the degradation process. To further verify the reactive oxygen radicals generated from the *E. coli*-Ag_2S QD biohybrid system under visible light irradiation, the ESR method using DMPO as a spin-trapping reagent was carried out. As depicted in Figure 4a,b no apparent $\bullet O_2^-$ signal can be

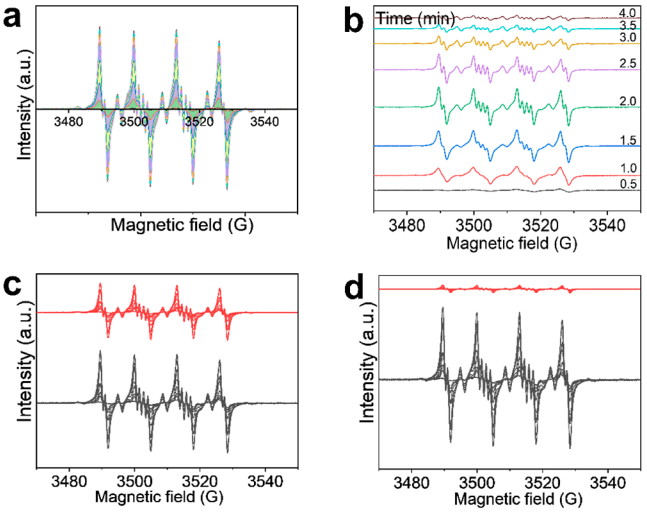

Figure 4. (a) ESR spectra of DMPO/$\bullet O_2^-$ in the presence of the *E. coli*-Ag_2S QD biohybrid system under visible light irradiation. (b) ESR spectra of DMPO/$\bullet O_2^-$ after 4 min visible light irradiation. (c) ESR spectra of DMPO/$\bullet O_2^-$ with different concentrations of Ag_2S QDs. Red lines represent 0.67 ± 0.03 μg Ag_2S QDs/10^8 cells, and black lines represent 0.96 ± 0.02 μg Ag_2S QDs/10^8 cells. (d) ESR spectra of DMPO/$\bullet O_2^-$ before (black lines) and after (red lines) the addition of SOD (3000 U L^{-1}).

detected in the ESR spectrum of the *E. coli*-Ag_2S QD biohybrid system under dark conditions, while the characteristic peaks (1:1:1:1) of $\bullet O_2^-$ are observed in the *E. coli*-Ag_2S QD biohybrid system under visible light irradiation, further demonstrating that $\bullet O_2^-$ is the key reactive oxygen radical during this reaction. In contrast, the characteristic peaks of DMPO/•OH (1:2:2:1) adducts were not observed under the same conditions (Figure S7). Moreover, we found that the signal intensity of DMPO/$\bullet O_2^-$ increased with the amount of the synthesized Ag_2S QDs (Figure 4c), indicating that the production of superoxide was directly related to the concentration of Ag_2S QDs. We also investigated the effect of SOD on the *E. coli*-Ag_2S QD biohybrid system as it can convert$\bullet O_2^-$ to O_2. The signal intensity of DMPO/$\bullet O_2^-$ quickly diminished after adding SOD (Figure 4d), indicating

https://doi.org/10.1021/acsanm.2c01955
ACS Appl. Nano Mater. XXXX, XXX, XXX−XXX

that $\bullet O_2^-$ plays a significant role in the photodegradation process.

The proposed photocatalysis mechanism by which the *E. coli*-Ag_2S QD biohybrid system degrades organic pollutants under visible light irradiation is shown in Scheme 1. Under visible light irradiation, electron−hole pairs are generated in the conduction band (CB) and valence band (VB) of the synthesized Ag_2S QDs. The band gap of the Ag_2S QDs is calculated to be 1.53 eV from the UV−vis-DRS spectrum (Figure S4b), which is higher than that of bulk Ag_2S (0.9 eV) due to quantum confinement effects.[39,40] Meanwhile, the potential values of CB and VB of Ag_2S QDs are calculated to be −0.31 eV (CB) and 1.22 eV (VB) according to previously reported formulas.[41,42] Due to the potential of $O_2/\bullet O_2^-$ (−0.28 eV vs. NHE), electrons with a potential of −0.31 eV transfer from the CB of Ag_2S QDs to O_2 to generate $\bullet O_2^-$. However, as the potential of $\bullet OH/H_2O$ (2.38 eV vs. NHE) is lower than the VB of Ag_2S QDs (1.22 eV vs. NHE), oxidative species (•OH) cannot be generated, which is consistent with the above mentioned ESR results. Instead, photogenerated holes in the VB degrade organic pollutants directly. The photogenerated electrons from the surface of Ag_2S QDs are quickly captured and react with the dissolved O_2 in the system to yield $\bullet O_2^-$, which in turn react with the organic pollutants to degrade the organic pollutants. Meanwhile, the photogenerated holes (h^+) accumulated in the VB of Ag_2S QDs further accelerate the degradation process, eventually resulting in clearly improved photocatalytic activity.

Scheme 1. Proposed Mechanism of Charge−Transfer Interaction and Photodegradation of Organic Pollutants with the *E. coli*-Ag_2S QD Biohybrid System Under Visible Light Irradiation

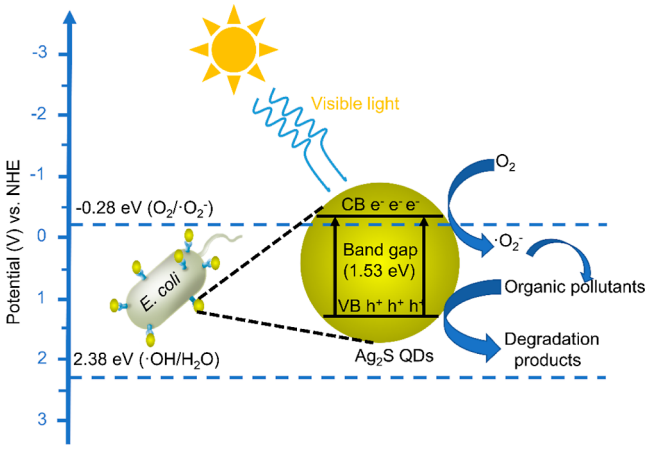

3.4. Biocompatibility of the *E. coli*-Ag_2S QD Biohybrid System. Although the efficient photocatalytic performance of the *E. coli*-Ag_2S QD biohybrid system was promising, reactive oxygen species produced in the photocatalytic degradation process may affect the biocompatibility of the biohybrid system. Cell surface-display system as a promising platform avoids possible poisoning of the biohybrid catalyst through the isolation of whole cells from the biohybrid catalyst displayed on the cell surface.[29,43] The cell membrane integrity and viability of the *E. coli*-Ag_2S QD biohybrid system during the photocatalytic processes were observed by fluorescent microscopy (Figure 5a,b). LIVE/DEAD BacLight viability kit was utilized to evaluate the viability of bacteria.[44] Compared to

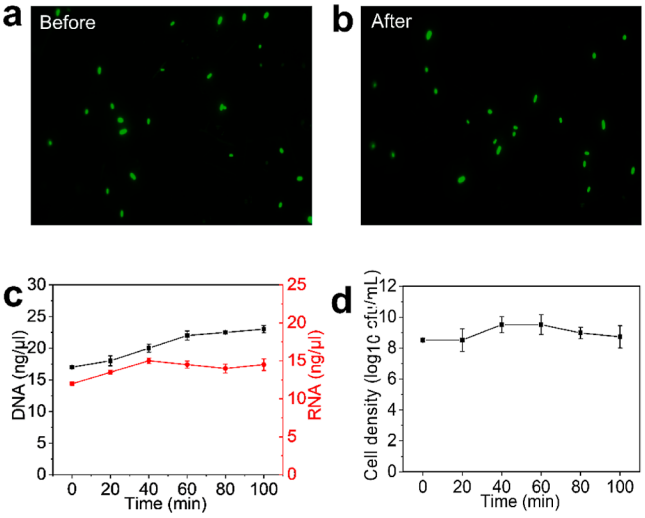

Figure 5. (a,b) Microscopic fluorescence images of the *E. coli*-Ag_2S QD biohybrid system before and after light exposure (scale bar: 20 μm). (c) Concentration of the leaked DNA and RNA during photocatalysis in the *E. coli*-Ag_2S QD biohybrid system. (d) Cell density of the *E. coli*-Ag_2S QD biohybrid system in the photocatalytic process.

damaged cells emitting red fluorescence,[45] cells with intact membranes exhibited green fluorescence, clearly indicating the cell membrane integrity. To further confirm this result, the leakage of DNA and RNA experiments was performed using a NanoDrop spectrophotometer, and the results showed no obvious leaked nucleic acids during the photocatalytic process (Figure 5c). Moreover, the cell viability of the *E. coli*-Ag_2S QD biohybrid system under visible light irradiation was investigated. As shown in Figure 5d, the cell population remained almost unchanged after 100 min, suggesting that the light intensity had no effect on cell growth. All these results demonstrated the excellent biocompatibility of the *E. coli*-Ag_2S QD biohybrid system to ensure its potential application in environmental remediation.

4. CONCLUSIONS

In summary, the *E. coli*-Ag_2S QD photosynthetic biohybrid system was successfully prepared based on a surface-display approach for the degradation of organic pollutants under visible light. The improved photocatalytic activity of the *E. coli*-Ag_2S QD biohybrid system is due to the effective separation and transfer of photogenerated charge of Ag_2S QDs. The photocatalytic mechanism indicates the key reactive species in degrading the organic pollutants under visible light irradiation. Furthermore, our results confirm that in situ synthesized Ag_2S QDs are capable of capturing light. This strategy could be extended to other well-established organisms, such as bacillus or yeast, to broaden its range of potential applications. Together, in addition to chemical and physical treatments, this biohybrid system based on bacterial surface-display technology provided an alternative approach for bioremediation of organic pollutants in aqueous environments.

■ ASSOCIATED CONTENT

Supporting Information

The Supporting Information is available free of charge at https://pubs.acs.org/doi/10.1021/acsanm.2c01955.

https://doi.org/10.1021/acsanm.2c01955
ACS Appl. Nano Mater. XXXX, XXX, XXX−XXX

SDS-PAGE and immunoblotting analyses, TEM, ICP-AES result, and near-infrared fluorescence imaging (PDF)

AUTHOR INFORMATION

Corresponding Authors

Kai Lin − *Jiangsu Environmental Resources Co., Ltd, Nanjing 210023, China*; Email: 368380386@qq.com

Wei Wei − *School of Life Sciences, Nanjing University, Nanjing 210023, China; Shenzhen Research Institute, Nanjing University, Shenzhen 518000, China; Nanchuang (Jiangsu) Institute of Chemistry and Health, Nanjing 210023, China;* orcid.org/0000-0003-0845-0527; Email: weiwei@nju.edu.cn

Jing Zhao − *State Key Laboratory of Coordination Chemistry, Chemistry and Biomedicine Innovation Center (ChemBIC), School of Chemistry and Chemical Engineering, Nanjing University, Nanjing 210023, China; Shenzhen Research Institute, Nanjing University, Shenzhen 518000, China; Nanchuang (Jiangsu) Institute of Chemistry and Health, Nanjing 210023, China;* orcid.org/0000-0001-5177-5699; Email: jingzhao@nju.edu.cn

Authors

Peiqing Sun − *State Key Laboratory of Coordination Chemistry, Chemistry and Biomedicine Innovation Center (ChemBIC), School of Chemistry and Chemical Engineering, Nanjing University, Nanjing 210023, China; Shenzhen Research Institute, Nanjing University, Shenzhen 518000, China; Nanchuang (Jiangsu) Institute of Chemistry and Health, Nanjing 210023, China*

Kunlun Li − *School of Life Sciences, Nanjing University, Nanjing 210023, China*

Complete contact information is available at: https://pubs.acs.org/10.1021/acsanm.2c01955

Notes

The authors declare no competing financial interest.

ACKNOWLEDGMENTS

This work was supported by the National Natural Science Foundation of China (22025701 and 22177048) and the Shenzhen Bay Laboratory Open Fund Project (SZBL2021080601013).

REFERENCES

(1) Kornienko, N.; Zhang, J. Z.; Sakimoto, K. K.; Yang, P.; Reisner, E. Interfacing nature's catalytic machinery with synthetic materials for semi-artificial photosynthesis. *Nat. Nanotechnol.* **2018**, *13*, 890−899.

(2) Zhang, J. Z.; Reisner, E. Advancing photosystem II photoelectrochemistry for semi-artificial photosynthesis. *Nat. Rev. Chem.* **2019**, *4*, 6−21.

(3) Cestellos-Blanco, S.; Zhang, H.; Kim, J. M.; Shen, Y.-x.; Yang, P. Photosynthetic semiconductor biohybrids for solar-driven biocatalysis. *Nat. Catal.* **2020**, *3*, 245−255.

(4) Hu, G.; Li, Z.; Ma, D.; Ye, C.; Zhang, L.; Gao, C.; Liu, L.; Chen, X. Light-driven CO_2 sequestration in Escherichia coli to achieve theoretical yield of chemicals. *Nat. Catal.* **2021**, *4*, 395−406.

(5) Su, Y.; Cestellos-Blanco, S.; Kim, J. M.; Shen, Y.-x.; Kong, Q.; Lu, D.; Liu, C.; Zhang, H.; Cao, Y.; Yang, P. Close-Packed Nanowire-Bacteria Hybrids for Efficient Solar-Driven CO_2 Fixation. *Joule* **2020**, *4*, 800−811.

(6) Honda, Y.; Shinohara, Y.; Fujii, H. Visible light-driven, external mediator-free H_2 production by a combination of a photosensitizer and a whole-cell biocatalyst: Escherichia coli expressing [FeFe]-hydrogenase and maturase genes. *Catal. Sci. Technol.* **2020**, *10*, 6006−6012.

(7) Honda, Y.; Shinohara, Y.; Watanabe, M.; Ishihara, T.; Fujii, H. Photo-biohydrogen Production by Photosensitization with Biologically Precipitated Cadmium Sulfide in Hydrogen-Forming Recombinant Escherichia coli. *Chembiochem* **2020**, *21*, 3389−3397.

(8) Xiao, K.; Tsang, T. H.; Sun, D.; Liang, J.; Zhao, H.; Jiang, Z.; Wang, B.; Yu, J. C.; Wong, P. K. Interfacing Iodine-Doped Hydrothermally Carbonized Carbon with Escherichia coli through an "Add-on" Mode for Enhanced Light-Driven Hydrogen Production. *Adv. Energy Mater.* **2021**, *11*, 2100291.

(9) Meng, S.-L.; Li, X.-B.; Tung, C.-H.; Wu, L.-Z. Nitrogenase inspired artificial photosynthetic nitrogen fixation. *Chem* **2021**, *7*, 1431−1450.

(10) Bellenger, J. P.; Darnajoux, R.; Zhang, X.; Kraepiel, A. M. L. Biological nitrogen fixation by alternative nitrogenases in terrestrial ecosystems: a review. *Biogeochemistry* **2020**, *149*, 53−73.

(11) Wang, B.; Xiao, K.; Jiang, Z.; Wang, J.; Yu, J. C.; Wong, P. K. Biohybrid photoheterotrophic metabolism for significant enhancement of biological nitrogen fixation in pure microbial cultures. *Energy Environ. Sci.* **2019**, *12*, 2185−2191.

(12) Sakimoto, K. K.; Wong, A. B.; Yang, P. Self-photosensitization of nonphotosynthetic bacteria for solar-to-chemical production. *Science* **2016**, *351*, 74−77.

(13) Honda, Y.; Hagiwara, H.; Ida, S.; Ishihara, T. Application to Photocatalytic H_2 Production of a Whole-Cell Reaction by Recombinant Escherichia coli Cells Expressing [FeFe]-Hydrogenase and Maturases Genes. *Angew. Chem., Int. Ed.* **2016**, *55*, 8045−8048.

(14) Wei, W.; Sun, P. Q.; Li, Z.; Song, K. S.; Su, W. Y.; Wang, B.; Liu, Y. Z.; Zhao, J. A surface-display biohybrid approach to light-driven hydrogen production in air. *Sci. Adv.* **2018**, *4*, No. eaap9253.

(15) Zhu, X.-G.; Long, S. P.; Ort, D. R. Improving Photosynthetic Efficiency for Greater Yield. *Annu. Rev. Plant Biol.* **2010**, *61*, 235−261.

(16) Xiao, K.; Liang, J.; Wang, X.; Hou, T.; Ren, X.; Yin, P.; Ma, Z.; Zeng, C.; Gao, X.; Yu, T.; Si, T.; Wang, B.; Zhong, C.; Jiang, Z.; Lee, C.-S.; Yu, J. C.-m.; Wong, P. K. Panoramic insights into semi-artificial photosynthesis: origin, development, and future perspective. *Energy Environ. Sci.* **2022**, *15*, 529−549.

(17) Giraldo, J. P.; Landry, M. P.; Faltermeier, S. M.; McNicholas, T. P.; Iverson, N. M.; Boghossian, A. A.; Reuel, N. F.; Hilmer, A. J.; Sen, F.; Brew, J. A.; Strano, M. S. Plant nanobionics approach to augment photosynthesis and biochemical sensing. *Nat. Mater.* **2014**, *13*, 530.

(18) Liu, S.; Tao, H.; Liu, Q.; Xu, Z.; Liu, Q.; Luo, J.-L. Rational Design of Silver Sulfide Nanowires for Efficient CO_2 Electroreduction in Ionic Liquid. *ACS Catal.* **2018**, *8*, 1469−1475.

(19) Zhang, Y.; Hong, G.; Zhang, Y.; Chen, G.; Li, F.; Dai, H.; Wang, Q. Ag_2S Quantum Dot: A Bright and Biocompatible Fluorescent Nanoprobe in the Second Near-Infrared Window. *ACS Nano* **2012**, *6*, 3695−3702.

(20) Hines, M. A.; Scholes, G. D. Colloidal PbS nanocrystals with size-tunable near-infrared emission: Observation of post-synthesis self-narrowing of the particle size distribution. *Adv. Mater.* **2003**, *15*, 1844−1849.

(21) Anikeeva, P. O.; Madigan, C. F.; Coe-Sullivan, S. A.; Steckel, J. S.; Bawendi, M. G.; Bulović, V. Photoluminescence of CdSe/ZnS core/shell quantum dots enhanced by energy transfer from a phosphorescent donor. *Chem. Phys. Lett.* **2006**, *424*, 120−125.

(22) Zimmer, J. P.; Kim, S.-W.; Ohnishi, S.; Tanaka, E.; Frangioni, J. V.; Bawendi, M. G. Size series of small indium arsenide-zinc selenide core-shell nanocrystals and their application to in vivo imaging. *J. Am. Chem. Soc.* **2006**, *128*, 2526−2527.

(23) Yang, H.-Y.; Zhao, Y.-W.; Zhang, Z.-Y.; Xiong, H.-M.; Yu, S.-N. One-pot synthesis of water-dispersible Ag_2S quantum dots with bright fluorescent emission in the second near-infrared window. *Nanotechnology* **2013**, *24*, 055706.

(24) Hong, G. S.; Robinson, J. T.; Zhang, Y. J.; Diao, S.; Antaris, A. L.; Wang, Q. B.; Dai, H. J. Vivo Fluorescence Imaging with Ag_2S

Quantum Dots in the Second Near-Infrared Region. *Angew. Chem., Int. Ed.* **2012**, *51*, 9818−9821.
(25) Du, Y.; Xu, B.; Fu, T.; Cai, M.; Li, F.; Zhang, Y.; Wang, Q. Near-infrared Photoluminescent Ag_2S Quantum Dots from a Single Source Precursor. *J. Am. Chem. Soc.* **2010**, *132*, 1470−1471.
(26) Liang, T.-Y.; Chan, S.-J.; Patra, A. S.; Hsieh, P.-L.; Chen, Y.-A.; Ma, H.-H.; Huang, M. H. Inactive Cu_2O Cubes Become Highly Photocatalytically Active with Ag_2S Deposition. *ACS Appl. Mater. Interfaces* **2021**, *13*, 11515−11523.
(27) Wei, W.; Liu, X.; Sun, P.; Wang, X.; Zhu, H.; Hong, M.; Mao, Z.-W.; Zhao, J. Simple Whole-Cell Biodetection and Bioremediation of Heavy Metals Based on an Engineered Lead-Specific Operon. *Environ. Sci. Technol.* **2014**, *48*, 3363−3371.
(28) Rebelein, J. G.; Cotelle, Y.; Garabedian, B.; Ward, T. R. Chemical Optimization of Whole-Cell Transfer Hydrogenation Using Carbonic Anhydrase as Host Protein. *ACS Catal.* **2019**, *9*, 4173−4178.
(29) Wei, W.; Zhu, T.; Wang, Y.; Yang, H.; Hao, Z.; Chen, P. R.; Zhao, J. Engineering a gold-specific regulon for cell-based visual detection and recovery of gold. *Chem. Sci.* **2012**, *3*, 1780−1784.
(30) Buxton, G. V.; Greenstock, C. L.; Helman, W. P.; Ross, A. B. Critical-Review of Rate Constants for Reactions of Hydrated Electrons, Hydrogen-Atoms and Hydroxyl Radicals (.Oh/.O-) in Aqueous-Solution. *J. Phys. Chem. Ref. Data* **1988**, *17*, 513−886.
(31) Wang, H.; Adesina, A. A. Photocatalytic causticization of sodium oxalate using commercial TiO_2 particles. *Appl. Catal., B* **1997**, *14*, 241−247.
(32) Schneider, J. T.; Firak, D. S.; Ribeiro, R. R.; Peralta-Zamora, P. Use of scavenger agents in heterogeneous photocatalysis: truths, half-truths, and misinterpretations. *Phys. Chem. Chem. Phys.* **2020**, *22*, 15723−15733.
(33) Hall Sedlak, R.; Hnilova, M.; Grosh, C.; Fong, H.; Baneyx, F.; Schwartz, D.; Sarikaya, M.; Tamerler, C.; Traxler, B. Engineered Escherichia coli Silver-Binding Periplasmic Protein That Promotes Silver Tolerance. *Appl. Environ. Microbiol.* **2012**, *78*, 2289−2296.
(34) Wang, B.; Zeng, C.; Chu, K. H.; Wu, D.; Yip, H. Y.; Ye, L.; Wong, P. K. Enhanced Biological Hydrogen Production from Escherichia coli with Surface Precipitated Cadmium Sulfide Nanoparticles. *Adv. Energy Mater.* **2017**, *7*, 1700611.
(35) Zhang, Y.; Liu, Y.; Li, C.; Chen, X.; Wang, Q. Controlled Synthesis of Ag_2S Quantum Dots and Experimental Determination of the Exciton Bohr Radius. *J. Phys. Chem. C* **2014**, *118*, 4918−4923.
(36) Meng, Z.-D.; Ghosh, T.; Zhu, L.; Choi, J.-G.; Park, C.-Y.; Oh, W.-C. Synthesis of fullerene modified with Ag_2S with high photocatalytic activity under visible light. *J. Mater. Chem.* **2012**, *22*, 16127−16135.
(37) Huang, S.; Tang, J.; Liu, X.; Dong, G.; Zhou, S. Fast Light-Driven Biodecolorization by a Geobacter sulfurreducens-CdS Biohybrid. *ACS Sustainable Chem. Eng.* **2019**, *7*, 15427−15433.
(38) Nosaka, Y.; Nosaka, A. Y. Generation and Detection of Reactive Oxygen Species in Photocatalysis. *Chem. Rev.* **2017**, *117*, 11302−11336.
(39) Rangappa, A. P.; Kumar, D. P.; Wang, J.; Do, K. H.; Kim, E.; Reddy, D. A.; Ahn, H. S.; Kim, T. K. In situ growth of Ag_2S quantum dots on SnS_2 nanosheets with enhanced charge separation efficiency and CO_2 reduction performance. *J. Mater. Chem. A* **2022**, *10*, 7291−7299.
(40) Yu, W.; Yin, J.; Li, Y.; Lai, B.; Jiang, T.; Li, Y.; Liu, H.; Liu, J.; Zhao, C.; Singh, S. C.; Chen, J.; Lin, B.; Idriss, H.; Guo, C. Ag_2S Quantum Dots as an Infrared Excited Photocatalyst for Hydrogen Production. *ACS Appl. Energy Mater.* **2019**, *2*, 2751−2759.
(41) Wu, Q.; Zhou, M.; Gong, Y.; Li, Q.; Yang, M.; Yang, Q.; Zhang, Z. Three-dimensional bandgap-tuned Ag_2S quantum dots/reduced graphene oxide composites with enhanced adsorption and photocatalysis under visible light. *Catal. Sci. Technol.* **2018**, *8*, 5225−5235.
(42) Ci, H.; Ma, L.; Liu, X.; Liang, Y.; Zheng, Y.; Li, Z.; Zhu, S.; Cui, Z.; Wu, S. Photo-excited antibacterial poly(ε-caprolactone)@MoS_2/ZnS hybrid nanofibers. *Chem. Eng. J.* **2022**, *434*, 134764.
(43) Grimm, A. R.; Sauer, D. F.; Polen, T.; Zhu, L.; Hayashi, T.; Okuda, J.; Schwaneberg, U. A Whole Cell *E. coli* Display Platform for Artificial Metalloenzymes: Poly(phenylacetylene) Production with a Rhodium-Nitrobindin Metalloprotein. *ACS Catal.* **2018**, *8*, 2611−2614.
(44) Zhang, Z.; Sun, J.; Chen, X.; Wu, G.; Jin, Z.; Guo, D.; Liu, L. The synergistic effect of enhanced photocatalytic activity and photothermal effect of oxygen-deficient Ni/reduced graphene oxide nanocomposite for rapid disinfection under near-infrared irradiation. *J. Hazard. Mater.* **2021**, *419*, 126462.
(45) Jiang, Z.; Wang, B.; Li, Y.; Chan, H. S.; Sun, H.; Wang, T.; Li, H.; Yuan, S.; Leung, M. K. H.; Lu, A.; Wong, P. K. Solar-light-driven rapid water disinfection by ultrathin magnesium titanate/carbon nitride hybrid photocatalyst: Band structure analysis and role of reactive oxygen species. *Appl. Catal., B* **2019**, *257*, 117898.

https://doi.org/10.1021/acsanm.2c01955
ACS Appl. Nano Mater. XXXX, XXX, XXX−XXX